Eur. Phys. J. D **9**, 105–110 (1999)

THE EUROPEAN PHYSICAL JOURNAL D

EDP Sciences
© Società Italiana di Fisica
Springer-Verlag 1999

Electronic and magnetic structure of artificial atoms

S.M. Reimann[1], M. Koskinen[1], J. Kolehmainen[1], M. Manninen[1], D.G. Austing[2], and S. Tarucha[3]

[1] Department of Physics, University of Jyväskylä, FIN-40351 Jyväskylä, Finland
[2] NTT Basic Research Laboratories, 3-1, Morinosoto Wakamiya, Atsugi-shi, Kanagawa 243-01, Japan
[3] University of Tokyo, Physics Department, 7-3-1 Hongo, Bunkyo-ku, Tokyo 113-0033, Japan

Received: 1 September 1998 / Received in final form: 21 October 1998

Abstract. The concept of shell structure has been found useful in the description of semiconductor quantum dots, which today can be made so small that they contain less than 20 electrons. We review the experimental discovery of magic numbers and spin alignment following Hund's rules in the addition spectra of vertical quantum dots, and show that these results compare well to model calculations within spin density functional theory. We further discuss the occurrence of spin density waves in quantum dots and quantum wires. For deformable two-dimensional quantum dots (for example, jellium clusters on surfaces), we study the interplay between Hund's rules and Jahn–Teller deformations and investigate the effect of magnetic fields on the ground-state shapes.

PACS. 71 Electronic structure – 73.20.Dx Electron states in low-dimensional structures – 85.30.Vw Low-dimensional quantum devices

1 Introduction

In solid-state physics, a beautiful analogy to shell structures and magic numbers in nuclei was found [1, 2] more than a decade ago: Sodium clusters with "magic" numbers of valence electrons appeared with enhanced abundance in the mass spectra. Following this discovery, much research focused on drawing analogies between such seemingly different systems as nuclei and metal clusters [3], and methods of nuclear physics were found useful for describing the electronic structure of such finite-sized samples of condensed matter. Today, one of the frontiers of condensed matter research is the study of low-dimensional nanometer-sized devices, with the aim of employing quantum electronics in technology [4]. Examples are the so-called bottom-up structures formed by self-organization of atoms and molecules into clusters and nanocrystals, and top-down structures created from larger pieces of materials by modern semiconductor processing techniques. Such man-made nanostructures confining a countable number of electrons are often called artificial atoms [5], because their electronic properties (for example, ionization or excitation energies) have many analogies to atomic physics. The most popular type of such devices are quantum dots, i.e., small electron islands artificially made from semiconductor heterostructures by lithography methods or etching techniques. Using electron beam lithography, metallic gates can be patterned on the surface of a heterostructure, such that the two-dimensional electron gas (2DEG) in the interface region of the different semiconductor materials beneath the gates is depleted, and the electrons are trapped in a conducting island. However, it is technically difficult to make the lithography very small. Most of the dots studied so far contain several hundred electrons and are more mesoscopic than microscopic quantum objects. Persson *et al.* [6] were among the first to show that the concept of a gross shell structure could provide a simple explanation of regular conductance oscillations, if one assumed tunneling through the quantum point contact barriers connecting the dot with the leads. A semiclassical approach using periodic orbit theory [7] (which had earlier been successful in explaining the shell- and supershell structure [8] in metal clusters) was found useful, as it allowed for a simple model of the more complicated many-particle problem in strong magnetic fields [9].

Besides the technical problems in their fabrication, gated quantum dots have other disadvantages when they are studied in very small systems: the tunnel barriers at the quantum point contacts, which are formed by the electrostatic depletion potential and connect the dots with the outer 2DEG become too large for a current to be observed [4].

Clear signals of shell structure in smaller systems as discovered recently [10] only became observable in experiments with vertical quantum dots, where the problem of large tunnel barriers could be avoided by the use double heterostructure barriers, which are more abrupt and thin [4]. Furthermore, the possibility of applying side gates around the mesa provided a much way of changing the dot size and geometry that was much more controlled than that using top gates for lateral structures. For such vertical dots, it was possible for the first time to probe the shell structure of an artificial atom with less than 20 electrons [10].

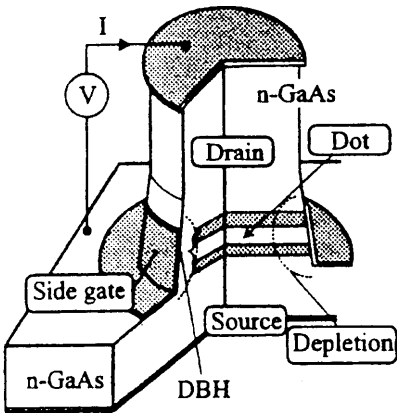

Fig. 1. Schematic diagram of a vertical quantum dot. From [10].

Shell fillings and the occurrence of Hund's rules have been reported earlier in both experimental [5, 6, 10] and theoretical [11–14] work. Here, we directly compare the measured addition spectra to results of spin density functional calculations (SDFT) [15] in the local spin density approximation (LSDA) and show that the experimentally observed shell gaps and the filling of single-particle levels following Hund's rules are in line with the theoretical results. We then extend our studies to deformed dots and quasi-one-dimensional (quasi-1D) quantum wires. We finally show that for deformable many-fermion systems (for example, metal clusters where the confinement is provided by a deformable charge background in which the delocalized valence electrons move), the ground-state symmetries are determined by Jahn–Teller deformations, which overcome Hund's rules, and we study the effect of magnetic fields on the symmetries of the ground states of quasi-two-dimensional electron gas clusters [16].

2 Shell structure in vertical quantum dots

A schematic picture of the gated vertical quantum dot used in [10] is shown in Fig. 1. The small conducting electron island forming the dot can be squeezed by a change in the voltage on a circular Schottky side gate around the structure. It is connected to the macroscopic voltage and current meters via the source and drain contacts. When the current as a function of the gate voltage was measured, current peaks were observed for each electron entering the dot. The spacing between two subsequent current peaks is proportional to the energy needed to add one more electron: This change in the so-called addition energy strongly depends on the number of particles already confined. Responsible for this are the electron–electron interactions, which become the more important the smaller the dot size is. Vertical quantum dots as described here have a disk shape with a thickness-to-diameter ratio of roughly 1:10 with a rather soft boundary [17]. One usually models such dots by a system of N electrons confined to a two-dimensional harmonic oscillator potential. At high densities, the kinetic energy dominates, and a model of independent electrons works reasonably well. The eigenspectrum of the two-dimensional oscillator potential $\varepsilon_n = \hbar\omega(n+1)$ has level degeneracies $d_n = n+1$, and thus magic shells are expected at the particle numbers $N = 2, 6, 12, 20, ...$ In the midshell regions, exchange effects become important, leading to spin alignment in degenerate single-particle orbitals following Hund's rules. To model the electronic structure of small dots, we have earlier applied density functional theory (DFT) in the local spin density approximation (LSDA) using the exchange-correlation functional of Tanatar and Ceperly [18]. (We refer to [12] for a more detailed description of the computational method used here). While most of the work on SDFT and Hartree–Fock calculations for circular quantum dots makes use of the azimuthal symmetry [19], we work in a plane wave basis, and thus our computational method avoids any symmetry restrictions for the solutions. The latter was found to be essential in accounting for spontaneously broken symmetries, e.g., spin density waves [12], and also allowed us to study noncircular dots.

2.1 Circular quantum dots

Consider now N electrons bound in the harmonic potential $V = m^*\omega^2(x^2+y^2)/2$, where m^* is the effective mass. The parameter $\omega^2 = e^2/(4\pi\epsilon_0\epsilon m^* r_s^3\sqrt{N})$ determines the average particle density $n_0 = 1/(\pi r_s^2)$ from the dot size N and the 2D Wigner–Seitz radius r_s. From the solution of the Kohn–Sham (KS) equations for different particle numbers and the choice of $r_s = 1.51\ a_B^*$ (corresponding to the equilibrium density of the two-dimensional electron gas), ground-state energies and densities were obtained. (We note that for full convergence, usually several hundred iterations of the KS equations were needed). In order to compare this to the experimental data, we calculated the effective atomic units for the energy $\mathrm{Ry}^* = m^*e^4/2\hbar^2(4\pi\epsilon_0\epsilon)^2$ and length $a_B^* = \hbar^2(4\pi\epsilon_0\epsilon)/m^*e^2$ using the dielectric constant $\epsilon \approx 13.1$ and effective mass $m^* = 0.067m_e$ in GaAs, which yields $a_B^* = 10.7$ nm and $\mathrm{Ry}^* = 5.31$ meV.

The addition spectra obtained experimentally from the current peak spacings can be theoretically modeled by the differences $\Delta_2(N) = \mu(N+1) - \mu(N)$ in the chemical potential $\mu(N) = E(N) - E(N-1)$. In the lower panel of Fig. 2, the solid line shows the addition energy changes obtained from the total ground-state energies calculated within the LSDA. The dashed line shows the experimental data [10] for a quantum dot with a diameter of about 0.5 μm. From this comparison, we see that the LSDA allows a surprisingly accurate estimate of the addition spectra. Both in the theoretical and experimental data, large amplitudes in $\Delta_2(N)$ are observed when the electron number coincides with a magic number $N = 2, 6$, or 12 of the single-particle two-dimensional harmonic oscillator. In the experimental data, however, no signals of a shell gap at $N = 20$ are seen [20]. In the midshell regions, we observe additional maxima at $N = 4$ and $N = 9$, and a less pronounced maximum in the experimental data at $N = 16$. Here, the total spin is nonzero, due to Hund's rule; this fa-

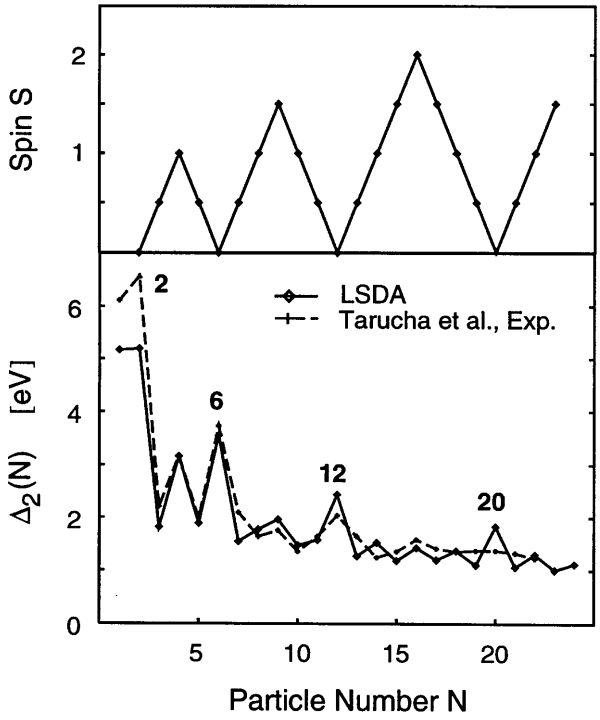

Fig. 2. Lower panel: Addition energy changes $\Delta_2(N)$ as a function of the electron number N for quantum dots with circular symmetry. Solid line: results from SDFT calculations; dashed line: experimental results from [10]. The numbers indicate the magic shell closures. Upper panel: Ground-state spin obtained within LSDA.

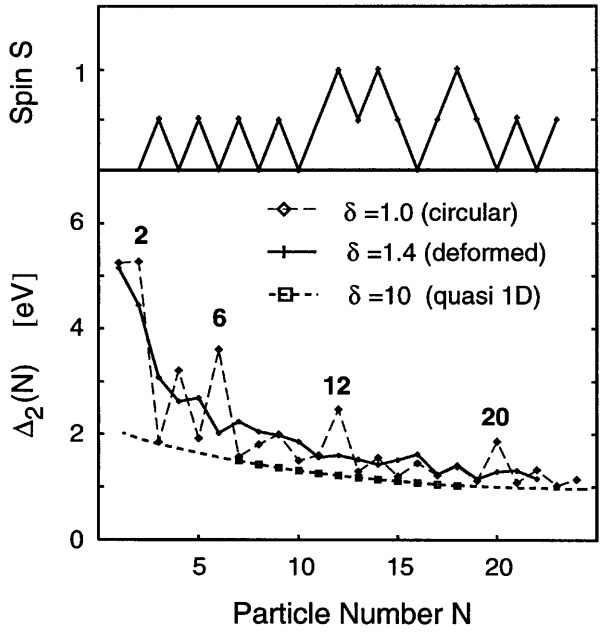

Fig. 3. Lower panel: Like Fig. 2, but for ellipsoidally deformed dots (solid line). The thin dashed line shows the results for circular dots for comparison. Also shown are the results for quasi-one-dimensional quantum wires without any shell structure (see Sect. 3). Upper panel: Total spin S.

vors large spins and thus magnetic states for electrons in degenerate, nonclosed shells.

The upper panel of Fig. 2 shows the total spin $S(N)$ as a function of particle number N obtained from the number difference of up-spin and down-spin particles. In the circular symmetric case, the function $S(N)$ is zero for the magic numbers and has maxima in the midshell regions.

Whereas the addition spectrum has the largest energy for $N = 2$, it gets strongly reduced for $N = 3$. The reason is the occurrence of spin degeneracy, that is, an unpaired spin in the highest occupied twofold degenerate orbital and total spin $S = 1/2$. Adding one more electron for $N = 4$ in the circular case, Hund's rule yields a total spin $S = 1$, since orbital degeneracy favors spin alignment in the highest occupied levels. For $N = 9$, the situation is very similar, yielding a total spin $S = 1\frac{1}{2}$.

Even without external magnetic fields, quantum dots show a rich variety of different magnetic ground-state structures: In dots with a larger number of electrons or a lower average electron density, states with nonuniform magnetization similar to spin density waves (SDW) first studied by Overhauser [21] can occur [12]. For the average density used in the calculation of the addition spectra in Fig. 2, such states are often found to have a slightly higher energy than the Hund state with nonzero total spin, but are ground states for, e.g., $N = 24$ and 34. Generally, depending on the value of r_s and the dot size N, there exists a critical value of the density where the SDW state sets in. The lower the average density is, the more ground states are found to be SDW states.

2.2 Deformed dots

We next study the shell structure and addition energies for anisotropic confinement $V(x, y) = m^*\omega^2(x^2\delta + y^2/\delta)/2$, where the deformation parameter δ is the ratio of the oscillator frequencies ω_x/ω_y and corresponds to the inverse ratio of semiaxes of the ellipsoid. The addition energies for $\delta = 1.4$ are shown in Fig. 3 (lower panel) together with the ground-state spin (upper panel) as a function of the dot size N. (The thin dashed line repeats the results for the circular dots for comparison.) One notices that the ellipsoidal deformation eliminates the magic shell closures at 2, 6, 12, and 20 as a simple consequence of broken symmetry. A similar reduction of the amplitudes in the addition spectra was also found for smaller deformations down to $\delta = 1.1$. Such deviations from perfect circular symmetry might explain why no pronounced shells could be seen for $N = 20$ in the experimental data [10] (cf. Fig. 1). We further observe that the odd–even oscillations in $\Delta_2(N)$ for the circular dots are far less pronounced in the deformed systems. From a comparison of the ground-state spins in the circular and deformed case (see upper panels of Figs. 2 and 3), we see that the total spin changes with deformation. For $N = 12$, which corresponds to a closed shell in the circular system, the spin has changed from the unpolarized $S = 0$ state to a Hund state with $S = 1$ in the elliptic confinement. Conversely, the spin in the midshell regions is now reduced, changing, for $N = 9$, from $S = 1\frac{1}{2}$ to $S = \frac{1}{2}$,

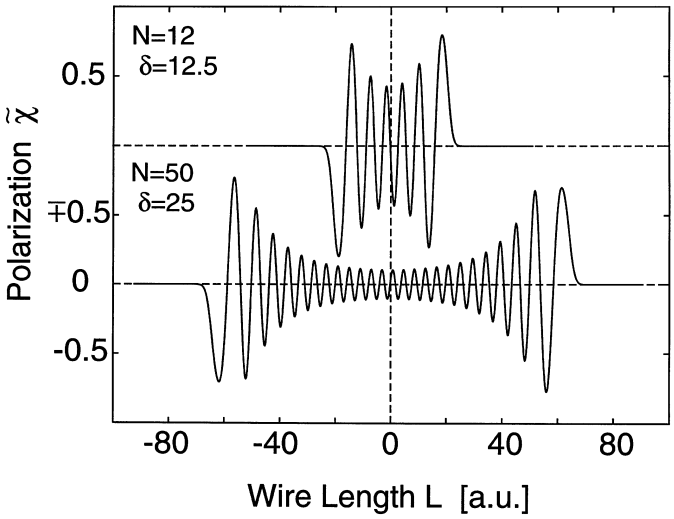

Fig. 4. Spin polarization in finite quantum wires with $N = 12$ and $N = 50$ electrons.

and for $N = 16$, from $S = 2$ to $S = 0$. The latter corresponds to a small-amplitude SDW ground state. For dots with magic shells, which are paramagnetic in the circular case, the deformation changes the ground state to a strong antiferromagnetic SDW with a large gap at the Fermi surface. A more detailed comparison to recent measurements of addition spectra for deformed dots [22] will be given elsewhere.

3 Quasi-one-dimensional electron systems

As the deformation gradually increases, the dots become quasi-one-dimensional: Along the shorter semi-axis of the deformed oscillator, the electrons occupy only the lowest states, whereas they can move freely in the direction of the longer axis. Such "superdeformed" dots resemble finite quantum wires.

The properties of interacting electrons in quasi-1D systems have been discussed much in connection with recent experiments on quantum point contacts (i.e., short constrictions connecting two electron reservoirs) made from heterostructures [23, 24] or small pillars of metallic material made by STM techniques (see [25] and references quoted therein). Special interest has been focused on the observation that depending on the width of the wires, the electron gas can polarize at rather large one-dimensional densities. From SDFT calculations, however, we found that before such Bloch instabilities occur, a spin–Peierls transition to a spin density wave state with antiferromagnetic order can be more energetically favorable [12].

Figure 4 shows for superdeformed quantum dots with 12 electrons at deformation $\delta = 12.5$, as well as 50 electrons at deformation $\delta = 25$, the normalized spin polarization $\widetilde{\chi} = (n^{\uparrow} - n^{\downarrow})/n_0$, plotted along the longer wire axis. (Here, $n^{\uparrow,\downarrow}$ labels the up- and down-spin density, respectively.) The polarization shows pronounced oscillations with an equal number of maxima and minima. Such an SDW with total spin resembles antiferromagnetic order and is characterized by a very large Fermi gap. The SDW causes a periodicity in the effective mean field potential. This can lead to localized end states [12] in a similar way to how surface states appear in a 3D lattice: The highest state is shifted into the Fermi gap, and the corresponding wave function is localized at both ends of the wire.

For even electron numbers, the total spin equals $S = 0$, and for odd electron numbers, it is $S = \frac{1}{2}$. In both cases, a large-amplitude SDW occurs. Due to the one-dimensionality, no shell gaps exist, and consequently the addition spectrum changes into a smooth curve (see lower panel of Fig. 3) when the system is gradually deformed towards a quasi-1D finite quantum wire.

4 Clusters on surfaces

Extensive studies of clustering processes of atoms on surfaces in recent years [26] have been motivated by the hope that nanostructures supported on surfaces could form a basis for the development of single-electron transistors and other quantum components. In a simple model for studying the electronic properties of such planar self-organized artificial atoms, one can neglect the interaction of the clusters with the surface and make use of the jellium model in its ultimate limit, assuming a fully deformable positive charge background, which compensates the charge density of the delocalized valence electrons.

4.1 Magic triangles in two-dimensional electron gas clusters

We have seen that spin effects and pronounced magic numbers are particularly strong for a rigid and highly symmetric confinement of the electronic system. In the ultimate jellium (UJ) model mentioned above, however, the electron gas is not subject to any external confinement, but can spontaneously break the symmetry; optimizing electronic structure such that the resulting shapes are deformed, and a gap is opened at the Fermi surface.

We have earlier studied the shapes of quasi-2D planar metal clusters in the UJ approach and found that for 2D clusters with magic shells $N = 6, 12, 20$, and 30, triangular symmetries are preferred. An example of the density for these triangular ground states is shown in panel (a) of Fig. 5 for $N = 30$. Between the magic shell closings corresponding either to circular or triangular geometry, strong Jahn–Teller deformed ground-state shapes were found [16]. Spontaneous symmetry breaking, which minimizes the degeneracy at the Fermi surface by opening a gap, seems to be energetically more favorable than retaining the symmetry and aligning the spins, or setting up a spin density wave. This result is supported by the observation that no states with nonuniform magnetization were found in any of the cases studied within the ultimate jellium model in zero magnetic fields.

The shell structure of planar clusters with 6, 12, 20, and 30 electrons suggests that such systems could be rather

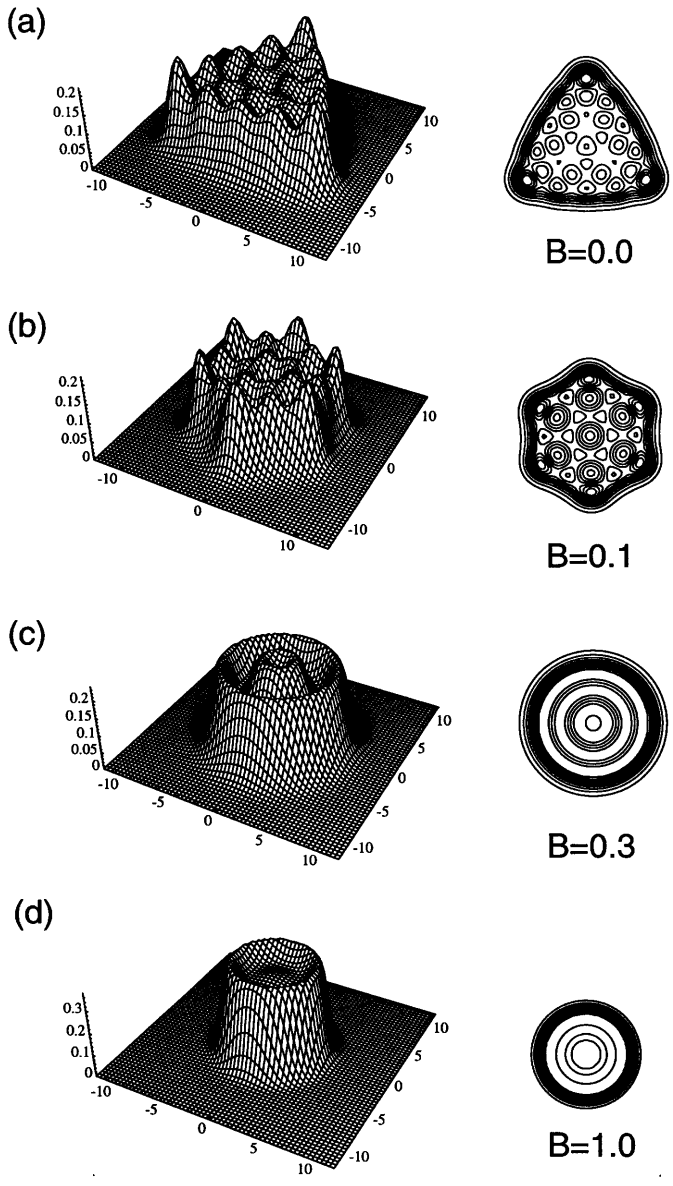

Fig. 5. Ground-state densities $n(x, y)$ and their contours for an ultimate jellium cluster with $N = 30$ electrons in magnetic fields perpendicular to the xy plane. Magnetic fields and length scales are in atomic units.

stable. Recently, Lai and Wang [27] have deposited gallium on the hexagonal surface of silicon. Using tunneling microscopy techniques, they observed a clustering process in the growth pattern of the gallium layer. Surprisingly, the gallium clusters showed a strong tendency to have triangular shapes, and a clustering of 10 atoms in a regular triangle seems to be the most abundant pattern. The formation of the gallium clusters is governed by interactions with the substrate, geometrical effects, and electronic structure. The hexagonal packing of atoms in the two-dimensional gallium layer should lead to the formation of either hexagons or equilateral triangles. Lai and Wang [27] have pointed out that the triangular shape yields a smaller number of dangling bonds on the silicon surface than the hexagonal shape and is thus preferred. Considering the electronic structure, one could now speculate that shell effects might support the triangular geometry in the cluster formation process: In the 10-atom gallium cluster, 18 of the valence electrons are needed to saturate the dangling bonds of the silicon surface. This would leave 12 free electrons corresponding to the magic number 12 for the triangular electron gas clusters discussed above.

4.2 Effect of magnetic fields on the shell structure of triangular 2D clusters

We next study the effect of a magnetic field on the shape and density distribution of triangular clusters. Vignale and Rasolt [28] developed the so-called current spin density functional theory (CSDFT), which includes the effect of orbital currents and provides a method for describing interacting fermions in a gauge field. This formalism was applied by various groups [14, 19] to describe quantum dot spectra in magnetic fields under the assumption of rotational symmetry. We refer to the contribution of Koskinen *et al.* [29] in these proceedings for a more detailed description of the CSDFT method for systems with broken symmetry, and comment here only on the effect of a magnetic field on the triangular UJ clusters. When applying a weak magnetic field, the resulting modifications in the single-particle energies and eigenfunctions let us expect that the clusters change their symmetry. We first study the triangular UJ cluster with six electrons. As the field is increased from zero, the ground state retains its symmetry, until at about $B = 0.4$ a.u., the shape changes to a stadium-like geometry. (In the following, we give the magnetic field in atomic units, where 1 a.u. = 6.86 T.) For fields larger than 0.6 a.u., the shape then changes to circular symmetry. (The cluster becomes polarized only for extreme fields above $B > 8$ a.u.) For 30 electrons, the situation is quite similar, with the only difference being that the larger particle number allows a larger variety of different shapes as the magnetic field is gradually raised. Again, in zero fields the ground state is triangular (see panel (a) of Fig. 4). Up to $B = 0.025$ a.u., the shape changes to a stadium-like geometry, and isomers of different shapes occur. At $B = 0.1$ a.u. (see panel (b) of Fig. 5), the shape changes to a regular hexagon. Finally, for $B \geq 0.3$ a.u., only circular shapes were found. From the density profiles shown in panel (c) for $B = 0.3$ a.u. as an example, one notices that the azimuthally symmetric droplets show radial oscillations in the density. The angular momentum is raised to the integer value $L = 114$. For even larger fields, the density in the middle of the dot becomes more homogeneous, and the system gradually develops into a state quite similar to the so-called maximum density droplet [30] for both spins $\sigma \in \{\uparrow, \downarrow\}$, where angular momentum is a good quantum number and the lowest momenta $l = 0, 1, 2, ..., (N^\sigma - 1)$ for each spin are occupied. (Here, N^σ labels the number of up- and down-spin particles, respectively). This is in agreement with the observation that the total angular momentum in this case equals $L = 210$. From (c) and (d) in Fig. 5, we see that the system size shrinks with increasing field: The charge-compensated electron gas retains the filling factor $\nu = 1$ for each spin direction because of the

increase in density. Consequently, fractional filling factors would not be accessible in the fully charge-compensated ultimate jellium model.

5 Conclusions

We have seen that shell structure, as it occurs in three-dimensional finite fermion systems, such as atoms, nuclei, and metal clusters, also can be observed [10] in the addition spectra of small vertical quantum dots. The experimental data were found to agree well with the description in the SDFT framework. This demonstrates the great reliability of the local density approximation, as is also known from its applications in atomic physics.

At about the equilibrium density of the 2DEG, the magic numbers in the finite system correspond to those of the noninteracting single-particle spectrum of the confining potential. Exchange becomes important only in the midshell regions. There, it systematically leads to spin alignment in degenerate single-particle orbitals following Hund's rules.

The electrostatic confinement of quantum dots is much more shallow than the $1/r$ Coulomb potential of the atomic nucleus. However, the important analogy to the physics of atoms has its origin in the fact that the electrons are confined by a *rigid* electrostatic potential. A metal cluster is much more similar to the nuclear case in the sense that Jahn–Teller deformations become important in the midshell regions. If the system is fully unconstrained in its geometrical symmetry, the Jahn–Teller effect seems to be a much stronger mechanism than spin alignment due to Hund's rules.

We thank Ben Mottelson and P.E. Lindelof for useful discussions. This work was financially supported by the Academy of Finland and the TMR programme of the European Community under contract ERBFMBICT972405.

References

1. W. Ekardt: Phys. Rev. B **29**, 1558 (1984)
2. W. Knight *et al.*: Phys. Rev. Lett. **52**, 2141 (1984)
3. M. Brack: Rev. Mod. Phys. **65**, 677 (1993)
4. L.P. Kouwenhoven *et al.*: "Electron transport in quantum dots", in *Proceedings of the Advanced Study Institute on Mesoscopic Electron Transport*, ed. by L.L. Sohn, L.P. Kouwenhoven, G. Schön (1997)
5. M.A. Kastner: Rev. Mod. Phys. **64**, 849 (1992); Phys. Today **46**, 24 (1993); R.C. Ashoori: Nature **379**, 413 (1996)
6. M. Persson *et al.*: J. Phys. (Cond. Matter) **7**, 3733 (1995); Physica B **194**, 1273 (1994)
7. M. Brack, R. Bhaduri: "Semiclassical Physics", in *Frontiers in Physics*, ed. by D. Pines, vol. 96 (Addison, Reading, Massachusetts 1997)
8. H. Nishioka, K. Hansen, B.R. Mottelson: Phys. Rev. B **42**, 9377 (1990)
9. S.M. Reimann *et al.*: Z. Phys. B **101**, 377 (1996)
10. S. Tarucha *et al.*: Phys. Rev. Lett. **77**, 3613 (1996)
11. D. Pfannkuche, V. Gudmundsson, P.A. Maksym: Phys. Rev. B **47**, 2244 (1992); P. Hawrylak, D. Pfannkuche: Phys. Rev. Lett. **70**, 485 (1993); P.A. Maksym: Phys. Rev. B **53**, 10 871 (1996)
12. M. Koskinen, M. Manninen, S.M. Reimann: Phys. Rev. Lett. **79**, 1389 (1997)
13. T. Ezaki, N. Mori, C. Hamaguchi: Phys. Rev. B **56**, 6428 (1997); S. Nagaraja *et al.*: Phys. Rev. B **56**, 15 752 (1997); In-Ho Lee *et al.*: Phys. Rev. B **57**, 9035 (1998);
14. Y.H. Zeng, B. Goodman, R.A. Serota: Phys. Rev. B **47**, 15 660 (1992); O. Steffens, U. Rössler, M. Suhrke: Europhys. Lett. **42**, 529 (1998)
15. P. Hohenberg, W. Kohn: Phys. Rev. **136**, B864 (1964); W. Kohn, L.J. Sham: Phys. Rev. **140**, A1133 (1965); U. von Barth, L. Hedin: J. Phys. C **5**, 1629 (1972).
16. S.M. Reimann *et al.*: Phys. Rev. B **56**, 12 147 (1997); ibid., Phys. Rev. B **58**, 8111 (1998)
17. S. Tarucha *et al.*: Superlattices Microstruct. **18**, 121 (1995); D.G. Austing *et al.*: Semicond. Sci. Technol. **11**, 388 (1996)
18. B. Tanatar, D.M. Ceperley: Phys. Rev. B **39**, 5005 (1989)
19. M. Ferconi, G. Vignale: Phys. Rev. B **50**, 14 722 (1994); V. Gudmundsson, J.J. Palacios: Phys. Rev. B **52**, 11 266 (1995); M.I. Lubin, O. Heinonen, M.D. Johnson: Phys. Rev. B **56**, 10 373 (1997); O. Heinonen, J.M. Kinaret, M.D. Johnson: [Cond-Mat/97712168]; M. Pi *et al.*: Phys. Rev. B **57**, 14 783 (1998)
20. The deviations at $N = 14$ and around $N = 20$ might generally be due to deformation of the quantum dot, which already for very small distortions changes the shell structure for larger N considerably
21. A.W. Overhauser: Phys. Rev. Lett. **4**, 462 (1960); Phys. Rev. **128**, 1437 (1962); Phys. Rev. **167**, 691 (1968)
22. S. Tarucha *et al.*: Jpn. J. Appl. Phys. **36**, 3917 (1997)
23. K.J. Thomas *et al.*: Phys. Rev. Lett. **77**, 135 (1996)
24. C.-K. Wang, K.-F. Berggren: Phys. Rev. B **57**, 4552 (1998)
25. N. Zabala, M.J. Puska, R.M. Nieminen: Phys. Rev. Lett. **80**, 3336 (1998)
26. H. Brune: Surf. Sci. Rep. **31**, 121 (1998)
27. M.Y. Lai, Y.L. Wang: Phys. Rev. Lett. **81**, 164 (1998)
28. G. Vignale, M. Rasolt: Phys. Rev. B **37**, 10 685 (1988)
29. M. Koskinen *et al.*: contribution to these proceedings
30. A.H. McDonald, S.-R. Eric Yang, M.D. Johnson: Austr. J. Phys. **46**, 345 (1993)